International Journal of Chemistry and Technology

http://dergipark.org.tr/ijct

Research Article

3d TiO$_2$ modified with reduced graphene embed into polyvinyl alcohol: photoanode electrode for oxygen evolution reaction

Fatih TEZCAN[1],*, Didem DEMİR KARAKUŞ[1]

^{1}Tarsus University, Department of Chemistry and Chemical Process Technology, Vocational School of Technical Sciences at Mersin Tarsus Organized Industrial Zone, Mersin, Türkiye

Citation: Tezcan, F.; Demir, Karakuş, D. *Int. J. Chem. Technol.* **2023**, 7 (2), 189-196.

ABSTRACT

The photocatalytic hydrogen production from water splitting using solar energy is one of the promising trend research topics within the scope of green energy production. A photoelectrochemical set-up consists of photoelectrode materials that directly use photon energy to convert water to hydrogen and oxygen. The photoelectrodes are photoanode and photocathode materials n-type and p-type semiconductors, respectively. In this study, the 3D TiO$_2$ photoanode surface was modified by coating it with reduced graphene (rG) and added polyvinyl alcohol (PVA) gel. PVA synthetic polymer with thermal stability, mechanical stability and low cost was preferred to provide distribution of rG material on 3D TiO$_2$ active surfaces. In this context, different amounts of rG (2.5, 5, 10 and 20%, based on polymer weight) impregnated with PVA gel coated on the 3D TiO$_2$ semiconductor surface were investigated. The solar light absorption behaviour and molecular interactions of the different amounts of rG in PVA on 3D TiO$_2$ semiconductor were monitored by UV-vis and Raman spectrometer. A photocatalytic performance of photoelectrodes were conducted by Electrochemical Impedance spectroscopy (EIS), linear sweep voltammetry (LSV) and chronoamperometric measurement under 100 mW cm^{-2} solar light. Raman spectrum showed dispersion of RG in PVA. EIS measurement showed that the polarization resistance (Rp) increased in 3D TiO$_2$ (21201.0 Ω cm^2) with only PVA coating (22816.1Ω cm^2), while the addition of rG to PVA (5404.5 Ω cm^2) caused a decrease in Rp at the semiconductor/electrolyte interface under sunlight. Furthermore, LSV and chronoamperometric measurement concluded that the increased amount of rG added to PVA increased the photoresponse of 3D TiO$_2$ 2.23-fold to the limit rG value.

Keywords: Photoanode, water splitting, oxygen evolution reaction, reduced graphene, polyvinyl alcohol.

1. INTRODUCTION

Carbon emission has dramatically increased with mainly fossil-based energy consumption, and global warming has reached an irreversible level for our earth. Therefore, researchers have studied various potentials of zero carbon content raw material on energy production to turn back the unpleasant circumstance.[1–3] One of the most is hydrogen gas can be altered the dreadful condition in favour of humankind's photoelectrochemical hydrogen production by solar energy.[4,5] The eco-friendly process is produced zero CO$_2$ emission and it is enabled to use renewable solar energy resources. Photoelectrochemical cells (PECs) produce hydrogen with solar irradiation as a clean energy process and it can consist of various combinations such as electrode/photoanode, electrode/photocathode and photoanode/photocathode in

mild/alkaline electrolyte.[6,7] Honda and Fujishima first reported[8] TiO$_2$ nanocrystal photoelectrode on photoelectrochemical hydrogen production with solar irradiation. During past decades, numerous research has been performed to solve the drawbacks of TiO$_2$ including photocorrosion durability, high chemical/physical stability, improving absorption and active electron/hole transportation at the interfaces.[9–12] Unfortunately, both wide bandgap and inactive electron/hole transportation boundaries involve the main hindrance of TiO$_2$. Some surface modifications have led to the improvement of the photocatalytic activity of TiO$_2$ in the PECs for hydrogen production such as 2D and 3D architecture design. It can serve more active sides to perform photoelectrochemical processes under solar irradiation. The further active side on the 3D architecture design leads to the enhancement of photocatalytic current density in the PECs systems.

But it is limited photoresponse due to only solar light absorption at the Uv- visible region.

One of the problems solving could be the advancement of an active layer on TiO$_2$, that enables a considerable benefit in further electron transportation at the semiconductor/electrode interface. Graphene oxide (GO) and rG material have intense interest recently, due to higher charge carrier mobility (10^5 cm^2 Vs^{-1} at an ambient temperature) and thermal conductivity (up to ~5000 W mK^{-1}).[13] Therefore, in the literature, many papers have been published on applying graphene derivates on TiO$_2$ in PECs. [14–18] Pei and co-worker[19] investigated TiO$_2$ nanocomposite with reduced graphene oxide in photocatalytic hydrogen evolution as a photocatalyst material. They suggested rG serving the good of electron-sink and electron-transporting bridges among various TiO$_2$ nanoparticles. Nada et al.[20] reported that rG modified on TiO$_2$ and magnetite Fe$_3$O$_4$ with varying quantities for photo-degradation of tartrazine dye under solar light, and rG modified photocatalyst reached more than 95% of degradation of tartrazine. Furthermore, various procedures of rG/TiO$_2$ synthesis are available including sol-gel method[21] and solvothermal/hydrothermal method[22] and simple mixing method.[23] The simple mixing method can be only performed by sonication, consequently, it is contemplated to be the simplest technique employed for obtaining material. As graphene materials apply with polymer composites, it can be serving enhancements in the inhibit photocorrosion, stability the cycle life of electrodes and increase the electrochemical performance such as polypropylene, polypyrrole, polyamide, polylactic acid, etc. [24–26] Especially, polyvinyl alcohol (PVA) and rG materials application has offered to advantage such as homogeneity dispersed 2-D layers of rG within the polymer[27] and enhanced thermal stability[28] and outstanding interfacial architectural interactions[29]. However, PVA/rG has not been published as photoelectrode material in photoelectrochemical hydrogen production. Furthermore, the choice of rG - PVA polymer 3D TiO$_2$ uses together can be enabled the synergic effect by a material structure such as photocorrosion resistance, material homogeneity, 3D electrode design and faster electron pathway into electrode/electrolyte interface. In this study, hydrothermally synthesized 3D TiO$_2$ is coated with rG impregnated into PVA polymer, which consists of the novelty of the paper.

2. MATERIALS AND METHODS

2.1. Materials

Titanium (IV) butoxide (97%), titanium tetrachloride (99%), hydrochloric acid (37%), sodium sulphite (95%), acetone (99.5%), reduced graphene (99.9%), (ethanol (99.9%), phosphate buffer (99%), PVA with a molecular weight of 89.000-98.000 g/mol (99% hydrolyzed) were

used without further purification procedure. A fluorine-doped tin oxide (FTO, ~8 Ω/Sq) electrode was utilized as a substrate.

2.2. Methods

FTO was washed followed by using detergent, acetone, ethyl alcohol, and distilled water for 5 min, respectively. Synthesis of 3D TiO$_2$ was performed in two hydrothermal deposition steps. Firstly, the previously applied procedure[30] with some modifications. 1D TiO$_2$ on the FTO glass substrate was deposited hydrothermally in an autoclave. 15 mL concentrated HCl was mixed slowly with 15 mL of distilled water with vigorous stirring for 5 minutes. 0.5 mL of Titanium (IV) butoxide, was put in slowly. The deposition solution was poured into a teflon-lined (100 mL) stainless steel autoclave already arranged with three FTO (0.8 × 1.25 cm^2). TiO$_2$ deposition was conducted for 12 hours at 150 °C in a furnace. 1D TiO$_2$ electrodes were washed with distilled water and ethyl alcohol and dried out at 40 °C in a furnace, respectively. The samples were calcined for an hour at 500 °C in a muffle furnace. Secondly, 1D TiO$_2$ electrodes were put in a highly concentrated titanium tetrachloride solution for an hour at 100 °C in an autoclave. The deposition solution was obtained by mixing 15 mL of concentrated HCl with 15 mL of distilled water, and 0.3 mL of titanium tetrachloride was added step by step to the solution. The deposition solution was added to an autoclave with previously obtained TiO$_2$ and heated for 3 hours at 150 °C in a furnace. The electrodes were washed with distilled water and ethyl alcohol and dried out at 40 °C in a furnace. Lastly, samples were calcined for an hour at 500 °C in a muffle furnace.

The surface coating of 3D TiO$_2$ with blank PVA and different ratios of RG-added PVA was carried out by directly separating the solution prepared in gel form onto the photoanode surface. PVA solution was fixed at 10% (w/v) polymer concentration for all samples. The calculated amount of PVA was weighed and dissolved in distilled water at 90°C. RG was added at different amounts (2.5, 5, 10 and 20%, based on polymer weight) into the 1 mL of PVA solution and kept in a sonicate for homogeneous distribution. The homogeneous mixture obtained in gel form was carefully spread on the 3D surface of the photoanode and left to dry at room temperature before use. The samples obtained are named TiO$_2$/P for the blank PVA solution and TiO$_2$/P/G, TiO$_2$/P/G2, TiO$_2$/P/G3 and TiO$_2$/P/G4 for the PVA solutions containing increased amounts of RG, respectively.

The photoelectrochemical tests of the samples were carried out by a CHI analyser (Model: CHI 660D electrochemical). For solar light simulation, a solar simulator was used with 100 m Wcm^{-2} power density (Sunlight TM Solar Simulators; M−SLSS;).

Photoelectrochemical tests were performed into 0.1 M Na_2SO_3- 0.1 M phosphate buffer electrolyte. Linear sweep voltammetry (LSV) was performed between -0.4 V and 1.6 V vs. Ag/AgCl reference electrode at 5 mV s^{-1} scan rate under light. The electrochemical impedance spectroscopy (EIS) measurement was carried out between 10^5 and 10^{-1} Hz at 0.6 V bias potential (5 mV amplitude). The chronoamperometric measurements were conducted at 0.6 V bias potential for 5 minutes.

3. RESULTS AND DISCUSSION

3.1. Photoelectrode characterization

UV-Vis spectrometer was performed to insight solar light absorption behaviour of samples. Commonly, TiO_2 electrodes absorb about 420 nm in the literature.[31,32] According to the UV-Vis spectrum, TiO_2 photoelectrode absorbs approximately 420 nm. Furthermore, TiO_2/P and various $TiO_2/P/G$ electrodes indicate similar absorption tendencies in the ultraviolet and visible regions. Therefore, it can be concluded that TiO_2 is a core thin film within samples. As compared TiO_2/P to RG-impregnated TiO_2/P electrodes, due to RG broad absorption, PVA is caused by decreasing absorption of TiO_2 due to characteristic absorption only ultraviolent.[33] However, inheritance of RG material induces enhanced light

absorption TiO_2/P during the visible region and $TiO_2/P/G3$ electrode reaches the greatest absorbance intensity, indicating boosted utilizing the solar light spectrum not only the ultraviolet region but also the visible region. Therefore, $TiO_2/P/G3$ can be an upper candidate photocatalytic electrode to OER under simulated solar irradiation. Consequently, photoelectrode band gap energy (E_g) is calculated by following the Tauc's equation.

$$(\alpha h\upsilon)^{1/r} = A\,(h\upsilon - E_g)$$

Herein, h is a Planck constant, α is the absorption coefficient, υ is frequency, r is the direct band transition ($r = 1/2$), and A is the experimental coefficient. The Uv-vis absorption curve converts to $(\alpha h\upsilon)^2$ versus $h\upsilon$. E_g value is obtained by extrapolating the curve to the x-axis of the curve drawing, and Tauc's plots are shown in Figure 1 (b). The calculated E_g values 3.06, 3.08, 3,06, 3.06, 3.03 and 3,04 of TiO_2, TiO_2/P, $TiO_2/P/G$, $TiO_2/P/G2$, $TiO_2/P/G3$ and $TiO_2/P/G4$, respectively. It indicates that all sample E_g values are close to each other and $TiO_2/P/G3$ electrode is the lowest E_g value. Therefore, we suggest that PVA and rG into PVA layers only perform slight alternation on E_g of the TiO_2 electrode.
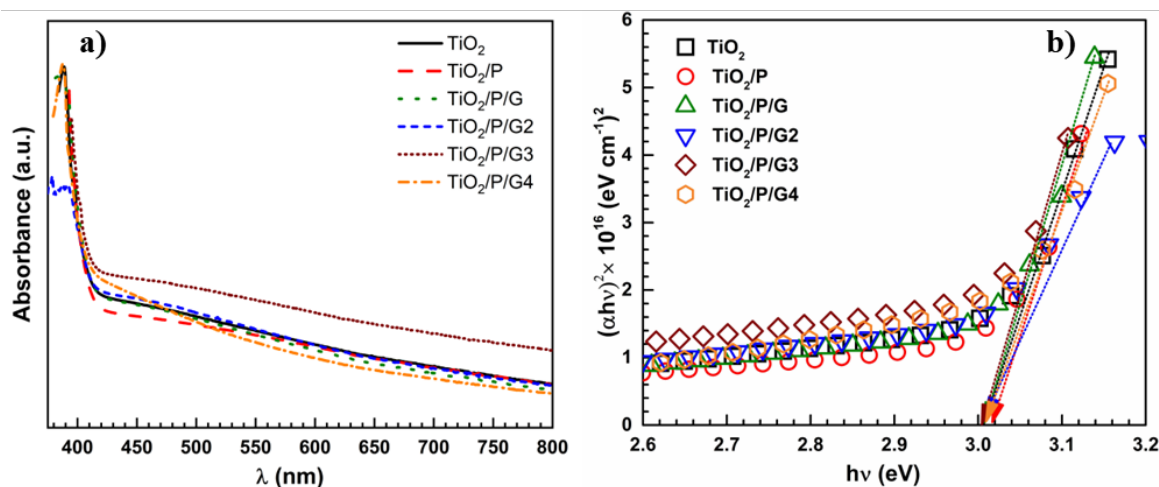
Figure 1. UV-Vis Spectrum (a) and Tauc plot (b) of 3D TiO_2, TiO_2/P, $TiO_2/P/G$, $TiO_2/P/G2$, $TiO_2/P/G3$ and $TiO_2/P/G4$.

To define photoelectrode composition structure, Raman spectrometer measurement was performed between 350 and 3200 cm^{-1} wavenumbers as shown in Figure 2. The Raman spectrum shows that the TiO_2 electrode gives three main distinctive peaks at about 234, 444, and 608 cm^{-1} which conforms to the tetragonal rutile phase TiO_2 of B_{1g}, E_g, and A_{1g}, respectively. [34] Both E_g and A_{1g} correspond to the Raman active main mode, while B_{1g} mode relates to multiple phonon vibration.[35]. Therefore, it can be suggested that characteristic rutile phase TiO_2 coated on FTO substrate. In addition, as seen in Figure 2, for Raman molecule stretching of PVA, is a strong peak

at 2921 cm^{-1}, corresponding to the stretching vibrations of $-CH_2$.[36] The Raman spectra of the various $TiO_2/P/G@$ shows two peaks at 1359 and 11605 cm^{-1} match with the D and G bands, respectively.[37] As the D band is related to disorder subsequent defects of structural, the G band is ascribed to the ordered domains of sp^2 carbon.[38] It could be concluded that rG material successfully dispersed the 3D TiO_2 surface with the help of PVA. The photoelectrode crystal structure and phase index were measured by X-ray diffraction. The XRD pattern of all samples is given in Figure 3. The 2θ° values of 3D TiO_2 sample indicate at 27.42°, 36.07°, 41.25°, 54.35°, 62.74°,

65.44°, and 68.92°, which conform hkl parameters to (110), (101), (111), (211), (002), (221) and (301), respectively. Accordingly, a 3D TiO_2 crystal structure can be called a tetragonal rutile phase (Reference code: 98-016-8140).[39] A hkl of (002) peak shows that the 3D TiO_2-grown mechanism conducts perpendicularly on the FTO glass substrate. As seen in Figure 3, included PVA 3D TiO_2 photoelectrodes indicate a broad peak at the 20.01° conformed hkl parameters to (101) plane of the semi-crystalline PVA.[40,41] In addition, RG the (002) plane shows at $2\theta°$ of 21.1°.[42] It can be concluded that both PVA and RG $2\theta°$ values overlap ranging 19.0 from 21.5.[43]
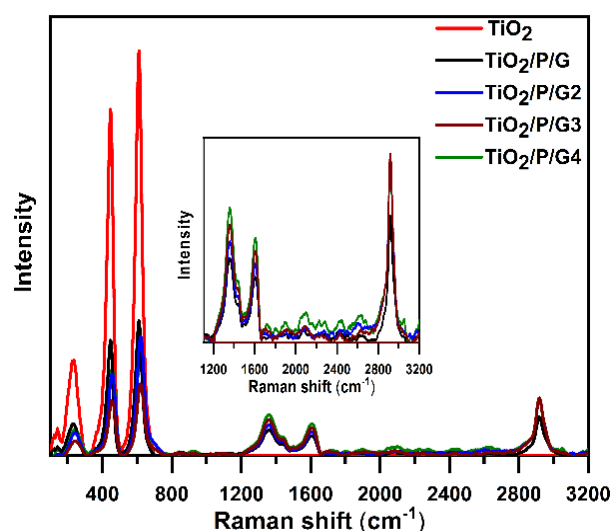
Figure 2. Raman spectrum of 3D TiO_2, TiO_2/P/G, TiO_2/P/G2, TiO_2/P/G3 and TiO_2/P/G4.
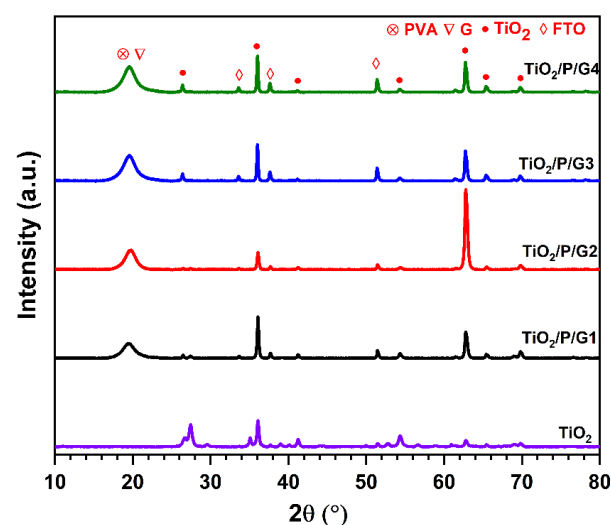
Figure 3. XRD pattern of 3D TiO_2, TiO_2/P/G, TiO_2/P/G2, TiO_2/P/G3 and TiO_2/P/G4.

3.2. Photocatalytic performance

The solar-driven water splitting process performs a photoelectrode/electrolyte interface, hence the photoelectrochemical conversion of H_2O to H_2 gas and O_2 gas should be taken into these boundaries. One of the most important is EIS measurement, which frequently has been utilized to define the durability of photoelectrode to photon energy and various resistances resources at the double layer.[44-46] EIS measurement was performed at 0.60 V bias potential with 5 mV amplitude under 100 mW cm^{-2} solar irradiation. Nyquist (a) and phase angle-frequency plots (b) of 3D TiO_2, TiO_2/P and various TiO_2/P/G@ photoelectrodes are given in Figure 4. As seen in the Nyquist plot, TiO_2 indicates a depressed loop at the low-frequency region, while TiO_2/P and various TiO_2/P/G photoelectrodes appear as two depressed loops at a high and low-frequency region. On the Nyquist plot, the semi-circle diameter magnitude is an indicator of the resistance supplies for OER under photon energy.

According to the Nyquist plot, two depressed loop diameters of the TiO_2/P photoelectrodes are higher compared with a depressed loop of TiO_2 electrode, indicating PVA layer increases resistance under solar light, due to the active sides of the 3D TiO_2 is hindered to OER process by PVA layer. However, TiO_2/P photoelectrodes photoresponse improved on the OER process with the addition of rG, resulting in depressed loops decreased by increasing rG loading into PVA. It suggests that impregnated rG into PVA causes enhancing electrical conductivity, absorption, and electron-transfer rate at the double layer. As a comparison of resistance of photoelectrodes, depressed loops are increased TiO_2/P>TiO_2>TiO_2/P/G>TiO_2/P/G2>TiO_2/P/G4>TiO_2/P/G3, respectively. It suggests that TiO_2/P/G3 photoelectrode performs the lowest resistance for the OER process under solar light, leading to further photo-assistant electrode structure on photoelectrochemical hydrogen production cell set-up. In addition, the phase angle-frequency plot indicates that the maximum phase angle of TiO_2/P shifts to the low-frequency region, related to causing PVA further film resistance for the OER process. Also, the extra loading of rG into PVA causes a decreasing maximum phase value such as TiO_2/P/G4. Consequently, the PVA layer leads to increasing resistance of TiO_2, but rG loading into PVA, which termination of negative phenomenon turns over to catalytic layer by increasing the conductivity of rG.

Zview software was used to obtain electrochemical parameters of photoelectrodes and the suggested electrical equivalent circuit of TiO_2, TiO_2/P and various TiO_2/P/G@ photoelectrodes are represented in Figure 4 (c) and (d), respectively. It indicates that R_s is a solution resistance (uncompensated resistance), R_{ct} is a charge transfer resistance at the high-frequency region, CPE_{ct} is a capacitance related to R_{ct}, R_f is a film resistance and

CPE_f is a capacitance related to R_f. In theory, EIS measurement investigates the photo-conversion of water to O_2 and H_2 gas with applied bias potential and photon energy photoelectrochemical at the semiconductor/electrolyte interface, called the Faradaic process. R_{ct} value is directly responsible to the Faradaic process on OER at the double layer. R_f relates with the PVA and rG impregnated into the PVA layer on the TiO_2 surface. Additionally, polarization resistance (R_p) sums up all resistance ($R_p = R_{ct} + R_f$) on the photoelectrode on OER. According to Table 1, the R_{ct} dramatically

decreased through coating PVA and rG impregnated into the PVA layer, indicating an enhanced Faradaic process owing to increasing conductivity of rG into PVA layers, resulting in improved electron transfer into semiconductor/electrolyte boundary. In comparison to R_f, rG significantly reduces R_f resistance source, due to conductive rG sheets enabling further OER process instead of only a lower conductive PVA layer. Furthermore, $TiO_2/P/G3$ displays the lowest R_p, suggesting OER process semiconductor/electrolyte interface.
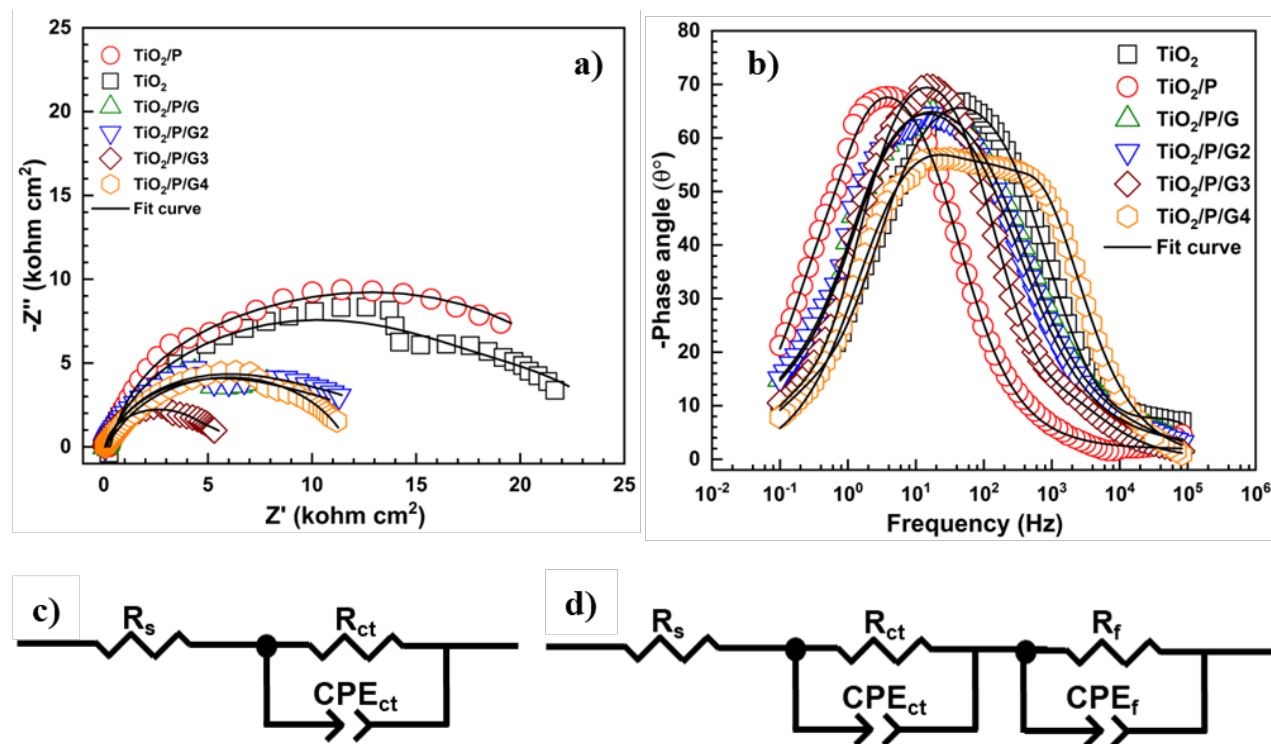
Figure 4. Nyquist (a) phase angle-frequency plot of TiO_2, TiO_2/P, $TiO_2/P/G$, $TiO_2/P/G2$, $TiO_2/P/G3$ and $TiO_2/P/G4$ into 0.1 M Na_2SO_3-0.1 M phosphate buffer under 100 mW cm^{-2} solar light. The suggested electrical equivalent circuits of TiO_2 (c) and TiO_2/P, $TiO_2/P/G$, $TiO_2/P/G2$, $TiO_2/P/G3$, $TiO_2/P/G4$ (d) photoelectrodes.

Table 1. The calculated electrochemical parameters of photoelectrode.

Electrode	R_{ct} (Ω cm^2)	C_{CPEct} (Ω^{-1}s^{n}cm^{-2})×10^{-5}	R_f (Ω cm^2)	C_{CPEf} (Ω^{-1}s^{n}cm^{-2})×10^{-5}	R_p (Ω cm^2)
TiO_2	21201	0.627	-	-	21201.0
TiO_2/P	31.1	1.389	22783.0	2.355	22816.1
$TiO_2/P/G$	21.2	2.559	12390.0	2.445	12411.2
$TiO_2/P/G2$	17.6	0.795	11546.0	1.429	11718.6
$TiO_2/P/G3$	15.5	1.942	5389.0	2.920	5404.5
$TiO_2/P/G4$	17.0	11.602	11667.0	2.443	11684.0

The photoelectrochemical performance of samples were conducted under 100 mW cm^{-2} solar irradiation by LSV measurement Figure 5 (a) and chronoamperometry measurements Figure 5 (b). LSV plot shows that the OER process performs a range from 1.0 V to 1.3 V depending on photoelectrodes. Therefore, we propose the OER process accomplished at 1.2 V by bias potential and solar irradiation. The photocurrent density of samples are 0.101 mA cm^{-2}, 0.063 mA cm^{-2}, 0.086 mA cm^{-2}, 0.103

mA cm^{-2}, 0.277 mA cm^{-2} and 0.141 mA cm^{-2} for TiO_2, TiO_2/P, $TiO_2/P/G$, $TiO_2/P/G2$, $TiO_2/P/G3$ and $TiO_2/P/G4$, respectively. It indicates that the PVA layer causes decreased photoresponse of TiO_2 photoanode on solar-driven water splitting. It can be related to the photo inactive polymer of PVA, which only absorbs the light UV-vis region, decreasing electron transfer at the interfaces due to lower electrical conductivity. However, conductive layers of distinct rG lead improve

Int. J. Chem. Technol. **2023**, 7 (2), 189-196

Tezcan and Demir Karakuş

photocatalytic performance under solar light irradiation, resulting in enabling further electron transportation for water oxidation to oxygen gas. Furthermore, the photo-response of $TiO_2/P/G@$ electrodes dramatically alters with the integration of rG into PVA on TiO_2 electrode and $TiO_2/P/G3$ indicates the most photocatalytic electrode with applied bias potential. It can be concluded that impregnation of rG into PVA causes increasing in conductivity consequently further charge carriers impose surface to perform the OER process. To investigate the photocatalytic stability of samples on the OER process, chronoamperometry measurement was conducted at 0.6 V bias potential under solar irradiation. In Figure 5 (b), electrodes indicate that PVA layer leads to decreasing performance of TiO_2, but the addition of rG into PVA cause boosting photocurrent density of TiO_2. Moreover, as in the LSV results, the chronoamperometric plots suggest that $TiO_2/P/G3$ photoelectrode shows photocurrent density stability at the 0.6 V bias potential under 100 mW cm^{-2} solar light. It can be concluded that the optimum rG content in PVA polymer layer on TiO_2 is G3.
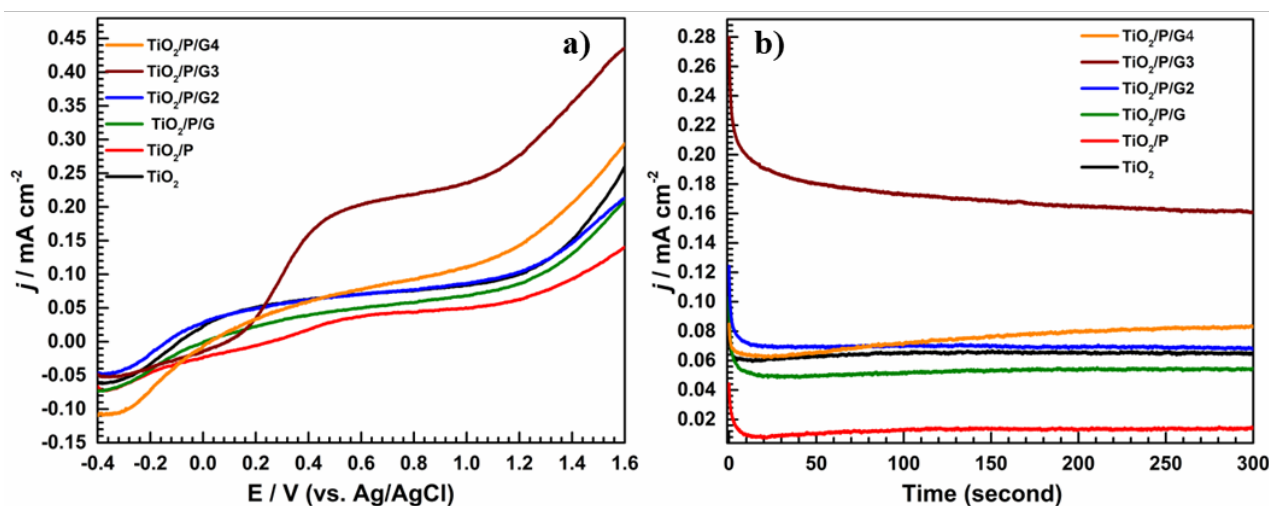
Figure 5. LSV (a) and chronoamperometry (b) TiO_2, TiO_2/P, $TiO_2/P/G$, $TiO_2/P/G2$, $TiO_2/P/G3$ and $TiO_2/P/G4$ into 0.1 M Na_2SO_3-0.1 M phosphate buffer under 100 mW cm^{-2} solar light.

4. CONCLUSION

In summary, a 3D TiO_2 surface coated with PVA solution containing different amounts of rG was successfully designed and obtained. The $TiO_2/P/G3$ photoelectrode indicated enhanced photocatalytic activity compared with TiO_2 and TiO_2/P photoelectrodes. The EIS results indicated that PVA layer increased R_p value of TiO_2 (22816.1Ω cm^2), but the addition rG into PVA on TiO_2 (5404.5 Ω cm^2) decreased the photoresistance of samples. According to LSV results, $TiO_2/P/G3$ photoelectrode displays a 2.23-fold photocatalytic response to TiO_2 under solar irradiation. rG impregnated into PV the A layer will be applied to a few semiconductors' materials for the PECs applications.

ACKNOWLEDGEMENTS

Conflict of interests

I declare that there is no a conflict of interest with any person, institute, company, etc.

REFERENCES

1. Li, H. X.; Moore, T.; Huang, J.; Zhang, P.; Costin, G. *Ener. Stra. Rev.* **2022**, 40, 100802.

2. Herrador, M.; de Jong, W.; Nasu, K.; Granrath, L. *Sci. Tot. Env.* **2022**, 820, 153274.

3. Chen, Q.; Kuang, Z.; Liu, X.; Zhang, T. *Appl. Ener.* **2022**, 312, 118744.

4. Acar, C.; Dincer, I. *Int. J. Hyd. Ener.* **2016**, 41, 7950-7959.

5. Hassan, N. S.; Jalil, A. A.; Khusnun, N. F.; Ahmad, A.; Abdullah, T. A. T.; Kasmani, R. M.; Norazahar, N.; Kamaroddin, M. F. A.; Vo, D. V. N. *Env. Chem. Let.* 2022, 1, 23.

6. Grimm, A.; de Jong, W. A.; Kramer, G. J. *Int. J. Hyd. Ener.* **2020**, 45, 22545-22555.

7. Chiu, Y. H.; Lai, T. H.; Kuo, M. Y.; Hsieh, P. Y.; Hsu, Y. J. *APL. Mater.* **2019**, 7, 8.

8. Fujishima, A.; Honda, K. *Nature.* **1972**, 238, 37-38.

9. Bashiri, R.; Samsudin, M. F. R.; Mohamed, N. M.; Suhaimi, N. A.; Ling, L. Y.; Sufian, S.; Kait, C. F. *Appl. Surf. Sci.* **2020**, 510, 145482 .

10. Bashiri, R.; Irfan, M. S.; Mohamed, N. M.; Sufian, S.; Ling, L. Y.; Suhaimi, N. A.; Samsudin, M. F. R. *Int J Hyd. Ener.* **2021**, 46, 24607-24619.

11. Wolcott, A.; Smith, W. A.; Kuykendall, T. R.; Zhao, Y.; Zhang, J. Z. *Small.* **2009**, 5, 104-111.

12. Dholam, R.; Patel, N.; Adami, M.; Miotello, A. *Int J Hyd. Ener.* **2008**, 33, 6896-6903.

13. Sun, Z.; Chang, H. *ACS. Nano*. 2014, 8, 4133-4156.

14. Zhu, S.; Song, Y.; Zhao, X.; Shao, J.; Zhang, J.; Yang, B. *Nano. Research*. 2015, 8, 355-381.

15. Hidayat, R.; Wahyuningsih, S.; Fadillah, G.; Ramelan, A. H. *J. Inorg. Organomet. Polym. Mater.* **2022**, 32, 1-9.

16. Li, W.; Zhang, H.; Chen, T.; Yang, L.; Sheng, C.; Wu, H.; Mao, N. *Tex. Res. J.* **2022**, 92, 5–6.

17. van Le, C.; Nguyen, M. T. T.; Le, N. T. T.; Le, H. K.; Bui, T. M.; Ho, D. H.; Le, V. H.; Ho, T. T. N.; Pham, T. L. C.; Huynh, L. T. N.; Nguyen, T. H.; Mai, T. P.; Hoang, N. M.; Nguyen, H. H. *Arab. J. Sci. Eng.* **2022**, 47, 1.

18. Kaur, H.; Kaur, S.; Kumar, S.; Singh, J.; Rawat, M. *J. Clust. Sci.* **2021**, 32, 1191-1204.

19. Pei, F.; Liu, Y.; Zhang, L.; Wang, S.; Xu, S.; Cao, S. *Mater. Res. Bull.* **2013**, 48, 2824-2831.

20. Nada, A. A.; Tantawy, H. R.; Elsayed, M. A.; Bechelany, M.; Elmowafy, M. E. *Solid. State. Sci.* **2018**, 78, 116-125.

21. Zhang, X. Y.; Li, H. P.; Cui, X. L.; Lin, Y. *J. Mater. Chem.* **2010**, 20, 2801-2806.

22. Pei, F.; Xu, S.; Zuo, W.; Zhang, Z.; Liu, Y.; Cao, S. *Int. J. Hyd. Ener.* **2014**, 39, 6845-6852.

23. Park, Y.; Kang, S. H.; Choi, W. *Phy. Chem.* **2011**, 13, 9425-9431.

24. Zhao, X.; Zhang, Q.; Chen, D.; Lu, P. *Macro.* **2011**, 44, 2392-2392.

25. Baig, U.; Uddin, M. K.; Sajid, M. *Mater. To. Commun.* **2020**, 25, 101534.

26. Pareek, A.; Paik, P.; Joardar, J.; Murugan, K.; Borse, P. H. *T. So. Fil.* **2018**, 661, 84-91.

27. Yang, X.; Li, L.; Shang, S.; Tao, X. *Polymer.* **2010**, 51, 3431-3435.

28. Liu, W.; Song, N.; Wu, Y.; Gai, Y.; Zhao, Y. *Vacuum.* **2017**, 138, 39-47.

29. Zhao, N.; Yang, M.; Zhao, Q.; Gao, W.; Xie, T.; Bai, H. *Inter. Arch. Eng.* **2017**, 11, 4777-4784.

30. Liu, B.; Enache-Pommer, E.; Aydil, E. S. *J. A.n Chem. Soc.* **2009**, 131, 3985-3990.

31. Alcudia-Ramos, M. A.; Fuentez-Torres, M. O.; Ortiz-Chi, F.; Espinosa-González, C. G.; Hernández-Como, N.; García-Zaleta, D. S.; Kesarla, M. K.; Torres-Torres, J. G.; Collins-Martínez, V.; Godavarthi, S. *Ceram. Int.* **2020**, 46, 38-45.

32. Liu, Y.; Li, R.; Yang, H.; Song, J.; Hu, J.; Yang, C.; Zheng, Z. *Int. J. Hyd. Ener.* **2022**, 47, 14563-14569.

33. Abdelghany, A. M.; Meikhail, M. S.; Abdelraheem, G. E. A.; Badr, S. I.; Elsheshtawy, N. *Int. J. Env. Stu.* **2018**, 75, 965-977.

34. Gao, X.; Liu, X.; Zhu, Z.; Wang, X.; Xie, Z. *Sci. Rep.* **2016**, 6, 30543.

35. Sun, Z.; Kim, J. H.; Zhao, Y.; Bijarbooneh, F.; Malgras, V.; Lee, Y.; Kang, Y.-M.; Dou, S. X. *J. Am. Chem. Soc.* **2011**, 48, 19314–19317.

36. Zubair, N. A.; Rahman, N. A.; Lim, H. N.; Zawawi, R. M.; Sulaiman, Y. *RSC. Adv.* **2016**, 21, 17720–17727.

37. Sharma, M.; Rani, S.; Pathak, D. K.; Bhatia, R.; Kumar, R.; Sameera, I. *Carbon. N. Y.* **2021**, 184, 437-444.

38. Ferrari, A. C.; Meyer, J. C.; Scardaci, V.; Casiraghi, C.; Lazzeri, M.; Mauri, F.; Piscanec, S.; Jiang, D.; Novoselov, K. S.; Roth, S.; Geim, A. K. *Phys. Rev. Lett.* **2006**, *97*, 187401.

39. Chen, J.; Song, W.; Hou, H.; Zhang, Y.; Jing, M.; Jia, X.; Ji, X. *Adv. Funct. Mater.* **2015**, *25*, 6793-6801.

40. Zhang, L. Z.; Wang, Y. Y.; Wang, C. L.; Xiang, H. *J. Memb. Sci.* **2008**, *308*, 198-206.

41. Shi, Y.; Xiong, D.; Li, J.; Wang, K.; Wang, N. *RSC. Adv.* **2017**, *7*, 1045-1055.

42. Gupta, B.; Kumar, N.; Panda, K.; Kanan, V.; Joshi, S.; Visoly-Fisher, I. *Sci. Rep.* **2017**, *7*, 45030.

43. Abu Hurayra–Lizu, K. M.; Bari, M. W.; Gulshan, F.; Islam, M. R. *Heliyon.* **2021**, *7*, 5.

44. Anantharaj, S.; Noda, S. *Chem. Electro. Chem.* **2020**, *7*, 2297-2308.

45. Bredar, A. R. C.; Chown, A. L.; Burton, A. R.; Farnum, B. H. *ACS. App. Ener. Mater.* **2020**, 3, 66-98.

46. Yang, W.; Moehl, T.; Service, E.; Tilley, S. D. *Adv. Ener. Mater.* **2021**, *11,* 2003569.